Overlapped Phased Array Antenna for Avalanche Radar

Mandana Ardeshir Tanha, Paul V. Brennan, Matthew Ash , Anselm Koehler, Jim McElwaine

***Abstract*—Snow avalanche is a natural phenomenon, which annually causes infrastructure damage and leads to human casualties in many countries all over the world. As a result, a detailed hazard mapping is required to be able to understand the avalanche risk levels. Also, the scarcity of the areas suitable for constructing infrastructures in the mountains places a high premium on providing high precision hazard mapping. This paper presents the design and development of an advanced phased array antenna for an FMCW radar to produce a high resolution image of snow avalanche in range and cross-range. The proposed antenna is a 16-element fully populated phased array with $\pm 14^{\circ}$ azimuth beamwidth and $\pm 22.5^{\circ}$ fixed elevation angle. The designed phased array antenna has 14.4dBi gain and -20.3dB sidelobe level. In this design Subarraying overlapping technique has been used to eliminate undesirable grating lobes by means of spatial anti-alias filtering. A phased array power divider is proposed to allow tapering of the amplitude of the elements to achieve low sidelobe level.**

***Index Terms*—Phased array, grating lobes, Overlapping Subarray, amplitude tapering, power dividers**

I. INTRODUCTION

SNOW avalanche is a significant threat to human life and infrastructure. Therefore, by risk assessment of the areas that are prone to avalanche, based on statistical analysis, the avalanche risk zones can be calculated. FMCW radar is an appropriate remote sensing tool that can be used to characterize the snow avalanche by transmitting chirp towards the target continuously. Such a radar requires an antenna with steering capabilities to be able to monitor the whole track of the snow avalanche. There are two basic choices of scannable antennas: mechanically scanned antennas and electrically scanned antennas [1]. With mechanically scanned antennas, beam agility is the function of motor speed/power and it takes around 1 s to scan all directions [1]. On the other hand, an electrically scanned antenna such as a phased array antenna can steer the beam in just a few microseconds [1]. Therefore, as a snow avalanche is a relatively fast moving target, an antenna with fast steering capability such as phased array antenna is required.

In designing the phased array antenna the unwanted grating lobes are the function of phased array inter-element spacing. Therefore, in the case where the inter-element is spacing is more than $\lambda/2$ to achieve the desired antenna beamwidth, a technique is required to be applied to suppress the grating lobes. There are several existing techniques which can be utilised to avoid grating lobes. One approach is to utilise Overlapped Subarrays based on Butler matrix [2]. The grating lobes can be also suppressed by amplitude tapering technique as shown in [3]. Other approach is to create randomly spaced Subarrays to eliminate the unwanted grating lobes as reported in [4]–[7]. Since subarraying technique gives rise to the phased array sidelobe level amplitude tapering technique is usually utilised to reduce the sidelobe level as reported in [3] and [8]. The amplitude of the phased array elements can be tapered by designing specific a feed network to assign the desired amount of power.

Developing a phased array antenna requires modelling of an array of radiating elements with a power distribution network to feed each array element. Then, by applying a relevant phase shift to each array element the phased array beam can be pointed to the desired direction [2]. The avalanche imaging FMCW radar receiver front-end receives the echo of the transmitted chirp and to produce the image of the avalanche by phased array multi-beam beamforming. In other words, the received echo by the phased array antenna is required to be multiplied by the all the complex weightings corresponding to the different beam angles to form a beam in that direction to be able to construct an image of the snow avalanche.

According to the existing literature there are various types of antenna that can be used as the radiating elements as reported in [9]–[12]. Among those, the microstrip patch antenna is a popular because of its low-profile and simple structure [13]. However, the microstrip patch antenna suffers from narrow bandwidth [7]. This problem can be tackled by applying several techniques such as using parasitic elements [14] and slot techniques [15]–[17]. Using parasitic elements can make the structure of the array much complicated, therefore loading the slot is a more convenient technique to enhance the bandwidth of the microstrip patch antenna.

As mentioned phased array antenna power distribution feed network design play a significant role in assigning the required amount of power to each phased array element. There are different types of phased array feed network that can be implemented, such as optical space feed, series feed and parallel feed [2]. The main drawback of the optical space feed is the reflection loss and low level of flexibility in controlling the pattern to achieve low sidelobe level [2]. Moreover, in the case that series feed network is utilized the path length to each radiating element is a function of frequency which limits the instantaneous bandwidth [2]. In contrast to the series feed network, parallel feed (i.e. corporate) is not dependent on the path lengths and it has a simple structure and it is composed of microstrip transmission lines and microstrip power dividers

Mandana Ardeshir Tanha is with the Department of Electrical and Electronic Engineering, University College London, London, United Kingdom e-mail:uceeard@ucl.ac.uk.

Paul Brennan is with the Department of Electrical and Electronic Engineering, University College London, London, United Kingdom e-mail:p.brennan@ucl.ac.uk.

Manuscript received October , 2016.

[2]. There are different types of power divider that can be used to split the power to the phased array elements such as Wilkinson power divider and T- junction divider.

In this paper a phased array antenna for an FMCW radar is presented. This system has the potential to produce high resolution snow avalanche images in two spatial dimensions. The proposed phased array antenna for the FMCW radar is a 16-element fully populated uniformly spaced antenna with a unique structure to achieve the required antenna beamwidth while suppressing unwanted grating lobes, utilizing an overlapping subarraying technique. Also, to reduce the phased array antenna sidelobe level 3dB power difference is required between the overlapping and non-overlapping elements. Therefore, it is required to use a power splitter to assign desired power to the overlapping and non-overlapping elements. There are several existing power dividers such as hybrid, directional coupler and Wilkinson power divider which can be used for such applications [18]. Among the aforementioned power dividers Wilkinson power divider has been widely used for phased array radar applications.Therefore, Diamond Two-in Two-out splitter is proposed which assigns the required amount of power to the overlapping elements to achieve the aforementioned power difference.In [19], a power distribution network was designed and simulated using Wilkinson power divider to assign required amount of power to the overlapping elements, however the reported structure can only be used in asymmetrical phased array configurations. Also, in [20] the Star-Wilkinson power divider structure was shown which can be used to feed the phased array overlapping elements, however, according to the structure of the aforementioned power splitter which consisted of isolation resistors the high loss and side-lobe was achieved. In this paper, the mathematical and theoretical analysis of the Diamond Two-in Two-out power splitter is proposed for the phased array power distribution network which consists of parallel transmission lines in a diamond orientation to feed overlapping element while 3dB power difference between the overlapping and non-overlapping is achieved and the unwanted grating lobes are suppressed in the phased array visible region. The proposed phased array system was deployed at the avalanche test site in Alps, Switzerland and by processing the data collected by the 16-element phased array the image of the snow avalanche was produced which shows the performance of the phased array antenna.

This paper is organized as follows. In section II the methods of designing the phased array antenna and phased array feed network are presented. In section III, the results of simulation and measurement of the prototype phased array antenna are shown. After discussion of methods and results in section IV, conclusions are presented in section V.

II. METHODS

A. phased array antenna structure

The phased array antenna proposed for the snow avalanche imaging radar is required to have 200 MHz bandwidth at 5.3 GHz centre frequency and $\pm 14^\circ$ beamwidth in azimuth and $\pm 22.5^\circ$ fixed elevation angle to enable the radar to record the avalanche flow from the whole track of the avalanche. There are several important parameters in designing a phased array antenna such as number of elements, inter-element spacing and beamwidth. The phased array antenna beamwidth is the function of number of elements. As known the phased array antenna gain drops by increasing the array steering angle. Therefore, by using a large number of elements, regularly spaced, the gain drop effect can be minimized [2]. Moreover, the phased array inter-element spacing plays a significant role to suppress the unwanted grating in the phased array visible area. In this paper, a 16-element fully populated, uniformly spaced phased array antenna is proposed. According to the array factor Equation (1) where N is the phased array number of elements, d is the phased array inter-element spacing, θ_0 is the scanning direction and λ is the wavelength, 2 inter-element spacing is required to achieve the aforementioned $\pm 14^\circ$ in azimuth. The array pattern plot shown in Fig. 1 indicates that 1.8° array beamwidth is achieved which is in agreement with theoretical analysis using Equation (2) where L is the aperture length and λ is the wavelength. It can be also seen that the grating lobe separation is 0.5 in $\sin\theta$ and the grating lobes are not visible in the array visible area -0.25$\prec\theta\prec$+0.25. It should be noted that in this case the progressive phase shift among the phased array elements is zero and the target is assumed to be at the position normal to the array. By processing the signals at the edge of the field of view at $+14^\circ$ or sin = 0.25, the array factor becomes as shown in Fig. 1. This figure indicates that a target at $+14^\circ$ would be aliased by the grating lobe to the direction -14°. The appearance of the grating lobe is due to the wide phased array inter-element spacing which allows the grating lobes to enter the phased array visible area. Thus, in order to suppress the undesired grating lobe the element pattern can be used as a spatial anti-alias filter. One approach to overcome this problem was to use sub-arraying technique which will be discussed in the following section.

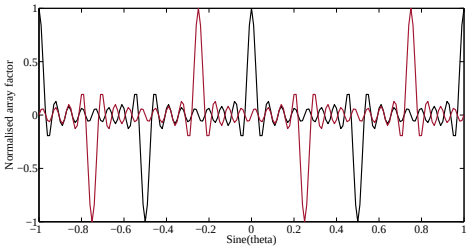

Fig. 1. Solid black line indicates the normalised array factor for the targets in the direction of array normal and 2λ is the array inter-element spacing. The main lobe appeared at $\sin\theta$=0. Solid red line shows the normalized array factor for the target at the edge of the field of view(+14°) of an array with 2λ inter-element spacing. The main lobe appeared at $\sin\theta = +0.25$ and the aliasing grating lobe appeared at $\sin\theta = -0.25$

$$E(\theta) = \frac{\sin\left(N\pi d/\lambda(\sin\theta - \sin\theta_0)\right)}{N\sin\left(\pi d/\lambda(\sin\theta - \sin\theta_0)\right)} \tag{1}$$

$$\Delta u = 0.88\lambda/L \tag{2}$$

1) Subarraying: Subarraying can be utilized by combining a number of elements spread over the inter-element spacing

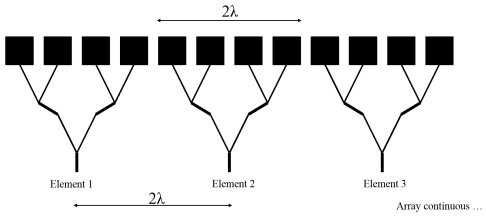

Fig. 2. Sub-arraying technique

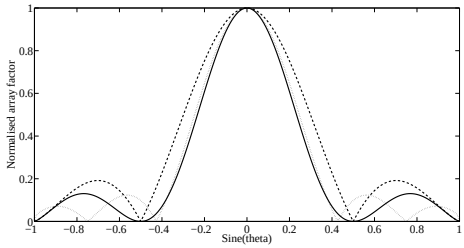

Fig. 3. Dashed line indicates non-overlapping four half wavelength spaced patches while dot line shows overlapping four half wavelength spaced patches and solid line illustrates overlapping four 2λ/3 spaced patches normalized array factor.

to act as a given array element [21]. One of the advantages of sub-arraying technique is that the antenna aperture size is increased and so higher gain and narrower beamwidth can be achieved. By using an overlapping technique in which antenna elements on the edges of sub-arrays are shared with adjacent sub-arrays, it is possible to control aliasing by achieving a narrower sub-array beamwidth than would normally be possible with a given sub-array spacing. This allows spatial anti-alias filtering to suppress grating lobes. Assuming four half-wavelength spaced elements in between the elements, then, the array element width becomes equal to the inter-element spacing as shown in Fig. 2. The array factor of such an array with four half-wavelength spaced element with the same weights assigned to each element is shown in Fig. 3. The result shows a reasonable anti-alias filter as the normalized array factor is -3dB at $\sin\theta$ = 0.25 but the sidelobe levels are rather high at -14dB. A more effective approach to suppress the grating lobes is to use an overlapping sub-array technique.

2) Overlapped Subarray: In the overlapped sub-array structure, each sub-array shares its outer elements with a neighbouring sub-array [21]. The overlapping technique thus increases the distance between the grating lobes while narrows down the phased array beamwidth. In other words, the overlapping allows a closer sub-array spacing in relation to the width of the sub-array. Therefore, by using this technique the phased array grating lobes may be suppressed from the visible region as the antenna beamwidth become narrower. To further decrease the sidelobe level, an amplitude tapering technique has been used at the expense of slightly broadening the main beam of the sub-array. As known, the array pattern, gain and sidelobe level are dependent on the average power radiated by each element therefore by assigning different weightings to each

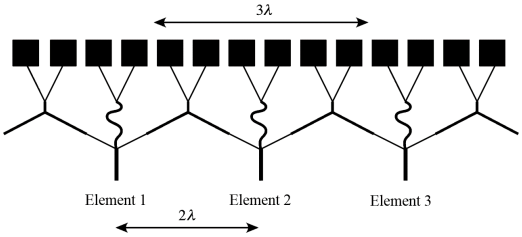

Fig. 4. Overlapping subarray with two shared elements

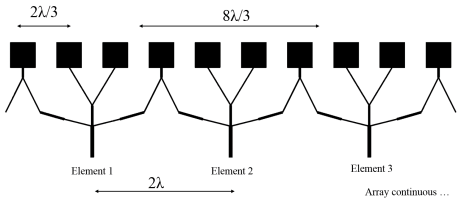

Fig. 5. Overlapping sub-array with one shared element

element the sidelobe level can be drastically reduced.

3) amplitude tapering: As an example, by using four half-wavelength spaced overlapping elements with [0.5, 0.5, 1, 1, 0.5, 0.5] weights (see Fig. 4), the array factor becomes as shown in Fig. 3. This is clearly an improvement over the previous result shown in Fig. 3 as the beamwidth is narrower and more capable of eliminating grating lobes corresponding to aliased targets and the lower sidelobe level achieved. The Array factor shows -6 dB at $\sin\theta$ = 0.25 and -18 dB sidelobe level. In an alternate design to suppress the grating lobes, the inter-element spacing within the sub-array elements can be derived using Equation (1) which in this case is 0.8λ, although for practical convenience a spacing of 2λ/3 has been chosen to allow use of uniformly spaced antenna in each two-wavelength interval, see Fig. 5. By applying [0.7, 1, 1, 0.7] weights to the elements within the sub-array the element pattern shown in Fig. 3 is achieved. In this case the element pattern has a narrower beamwidth with -20 dB sidelobe level.

4) elevation angle: According to the radar requirements the phased array antenna is required to have a fixed $\pm 22.5^{\circ}$ elevation angle. The elevation angle can be achieved by adding a second row of elements. The elevation spacing of the sub-array element can be derived using Equation (3) [22] , where in this equation de is the elevation inter-element spacing and $_e$ is the elevation angle. Assuming nominal array factor of -2 dB at the maximum elevation angle the spacing of 0.54λ is indicated. A value of 0.58λ is used in practice.

$$G(\theta_e) = \cos(\frac{\pi d_e \sin\theta_e}{\lambda}) \tag{3}$$

B. phased array antenna modelling

The phased array antenna designed based has been modelled in CST MICROWAVE STUDIO 2016. The first step to design the phased array antenna was to model a radiating element

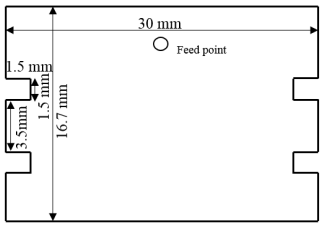

Fig. 6. Probe fed corrugated patch antenna dimensions

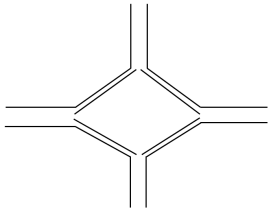

Fig. 7. Diamond Two-in Two-out splitter

to achieve the required antenna bandwidth with directional radiation pattern. Then, the phased array feed network was designed based on the weightings obtained in the previous sections. As there are several radars operating close to the centre frequency (5.3 GHz) of the proposed phased array radar, it was essential to design a bandpass microstrip filter to be able to reject the unwanted band of frequencies while having sufficient at attenuation at 5.8 GHz. Then, the phased array antenna prototype was developed in the University College London (UCL) workshop. Finally, after optimizing the phased array antenna model based on the results which will be discussed later, the final phased array design was fabricated by TrackWise manufacturer and the phased array antenna was installed at the avalanche test site at Valle‘e de Lassione, Switzerland.

C. radiating element design

The microstrip patch antenna structure was used as the phased array antenna radiating element because of its simplicity and low-profile. The microstrip patch antennas also have several disadvantages such as narrow bandwidth, spurious feed radiation and fabrication tolerances. Therefore, to be able to compensate for the aforementioned drawbacks a multilayer phased array structure was proposed. This structure consists of two double sided stacked substrates with a ground plane in the middle. The top radiating elements and antenna feed distribution network are mounted on 1.575 mm and 0.787 mm thickness Rogers/Duriod 5880 substrates with 2.2 dielectric constant and 0.009 loss tangent, respectively. The phased array radiating elements are mounted on the thicker substrate to increase the patch antenna bandwidth, as the amount of patch antenna fringing field in E-field (x-y plane) is dependent on the ratio of length to substrate height of the patch (L/h) and also the dielectric constant [22]. In other words the thick substrate extends the fringing field region. On the other side the feed network structure which will be discussed later was mounted on the thin substrate to avoid spurious feed network radiation. The corrugated patch antenna was designed for this application to achieve the required 200 MHz bandwidth. In [23], the right angle slots were placed at the non-radiating edges to extend the operation bandwidth by exciting two orthogonal modes on the patch antenna. In this application a similar approach has been used by inserting a very small corrugations at the non-effective length of the antenna to slightly increase the bandwidth of the patch antenna. The dimensions of the corrugated patch antenna are shown in Fig. 6.

D. feed network design

In this paper the corporate feed network, which consists of several microstrip transmission lines, is used to deliver the required power to the phased array elements. A corporate feed network is used as it is flexible and it is easier to develop for the cases where two dimensional array orientation is required [2]. As mentioned it was required to achieve 3 dB power difference between the phased array non-overlapping elements and overlapping elements. Clearly, in order to achieve this the half of the power at the centre of each sub-array should go towards the non-overlapping elements while a quarter of the power should go towards the non-overlapping elements. Therefore, to achieve 3 dB power difference between the overlapping and non-overlapping, the Diamond Two-in Two-out power splitter was proposed. The Diamond Two-in Two-out power splitter is a composed of four parallel microstrip transmission lines in series with Z0 characteristic impedance transmission lines in diamond orientation, see Fig. 7. The Diamond Two-in Two-out power splitter is a microstrip power divider which has four ports and divides quarter of the input power among its four points. Therefore,it can also be called 6dB power divider. The main advantage of the Diamond Two-in Two-out splitter is that it has a simple structure and resistors are not used in its structure in contrast to the existing four port power splitters such as Star Wilkinson power divider which is reported in [20] . Using resistors may cause having high sidelobe level and power loss.

Assuming P is the total amount of power which travels through the centre feed port, the half of the power goes through the non-overlapping elements and it further splits to half. As a result, the expected S21 (i.e. centre feed port and each overlapping element) value is -6dB. Ultimately, 1/16 of the total power reaches to each overlapping element. The diamond two-in two-out splitter has been designed both using lossy transmission line in CST and ideal transmission lines in MATLAB R2015a (Math Works,Inc.,Natick M, USA). The three- element phased array antenna using Diamond Two-in Two-out splitter and the corrugated patch antenna is shown in Fig. 8. This power divider was designed based based on optimisation to achieve the required amount of power at each port of the power splitter. Then, after that to justify the behaviour of the proposed power splitter, it was mathematically analysed based on transmission lines equations which will be shown in Discussion section. Appendix B also represents the transmission line impedances of the feed network.

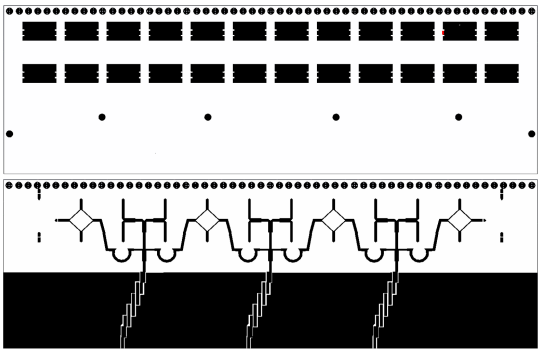

Fig. 8. Three element phased array antenna

E. Bandpass filter design

The parallel coupled lines can be used to easily construct different types of microstrip filters. Generally, the coupled line bandpass filters are used for applications which require less than 20% bandwidth [18]. The coupled line filter structure is shown in Appendix A. In the first place, the microstrip coupled line bandpass filter was designed individually on 0.787 mm Duriod 5880 by calculating the filter's parameters using fifth order normalized Chebyshev g-values with 0.5 dB passband ripple [18]. After that, the optimized coupled line bandpass filter was added to the feed point of the designed phased array antenna. The designed coupled line bandpass filter dimensions are shown in Appendix A.

F. phased array antenna prototype

The single-element phased array antenna was fabricated as a prototype. The designed phased array antenna fabrication was quite challenging as it was a multilayer structure and all the layers had to bond together without any air gap to avoid impedance mismatch. The phased array prototype was fabricated in cooperation with the UCL workshop. The finished board consists of four layers produced by gluing together two double-sided boards using LPKF "prepeg", which is an adhesive loaded FR4 with 2x100 microns thickness in a laminating press. Then the board was subsequently drilled and copper-plated and then finally both outer layers patterned by applying photoresist, UV-exposing a negative photo-film, developing the pattern and removing the unwanted copper by FeCI etching in a spray machine, see Fig. 9. After optimising the phased array antenna based on the prototype measurements, it was deployed outside the bunker at Valle'e De La Sionne (VDLS), Switzerland. The phased array antenna was installed outside the concrete wall of the bunker which was facing the mountain that was prone to avalanches and the radar transmitter was inside the bunker. An enclosure was also designed for the phased array antenna to be able to protect it.

III. RESULTS

A. phased array antenna return loss

The simulated phased array antenna return loss is compared to the measurement results. Fig. 10 illustrates that the single element of the phased array antenna has 400 MHz bandwidth

Fig. 9. Single element phased array antenna prototype. The top image shows the phased array feed network and the bottom picture indicates the phased array radiating elements

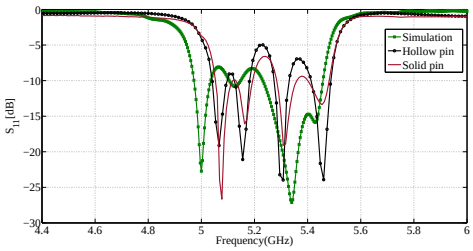

Fig. 10. Single phased array antenna simulation and measurement comparison

at -10 dB in simulation results. In the phased array antenna design solid pins were modelled to feed the patch antennas via transmission lines, but as mentioned to fabricate the phased array prototype through plating technique was used, therefore, it was required to fill all the through plate holes with solder to make the design similar to the original design. However, prior to that the antenna S_{11} was measured to be able to see how much it affects the return loss response. Fig. 10 compares the simulation results and measurement results. As it can be seen after filling the holes with solder there is up ward frequency shift compared to simulation results which can be due to the fabrication tolerances. Also, further investigation it was found the coupled line bandpass filter response has also an upward frequency shift which affected the phased array antenna return loss response as was modified by shifting its centre frequency 10MHz downward with wider bandwidth to compensate for fabrication tolerances.

B. phased array antenna radiation pattern

The radiation pattern of the phased array antenna was measured in the UCL anechoic chamber. Fig. 11 indicates a comparison between the phased array simulation and measurement results. It has been shown that the phased array antenna has a flat-topped directional radiation pattern with

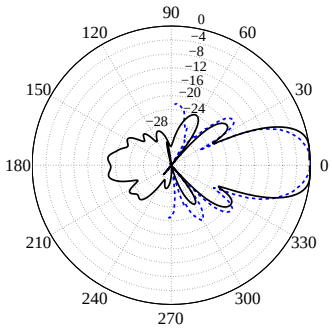

Fig. 11. Three element phased array prototype centre element radiation pattern at 5.3 GHz, ϕ=0. The dashed line shows the measurement results and the solid line indicates the simulation result

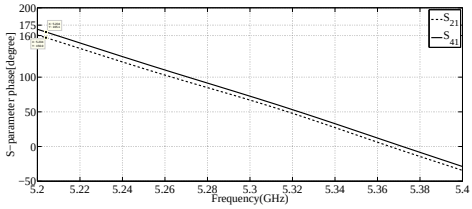

Fig. 12. According to Appendix C S_{21} and S_{41} show that the overlapping and non-overlapping elements are approximately in phase by maximum 10 ° difference.

-20.3 dB sidelobe level and 14.4 dBi gain in simulation. The reflection observed in the measurement results is due to imperfect orientation of the anechoic chamber.

C. phase matching

As mentioned in previous sections the phased the elements within the sub-arrays have to be in phase to avoid inconsistency in the array overall performance. As shown in previous section the sub-array elements are approximately in phase with 5° phase difference at most and exactly in phase at 5.3 GHz centre frequency. Therefore, after adding the Chebyshev coupled line bandpass filter to the antenna, the effect of the filter on the sub-array elements phase matching was investigated, see Fig. 12. As it can be realized the filter has negligible effect on the phase matching. Fig. 13 also indicates that by using Diamond Two-in Two-out power splitter 3dB power difference between overlapping and non-overlapping elements is achieved.

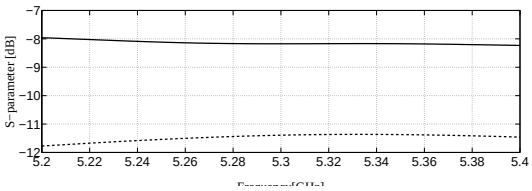

Fig. 13. According to Appendix C the magnitudes of S_{21} and S_{41} show that that there is 3dB power difference between the overlapping and non-overlapping elements.

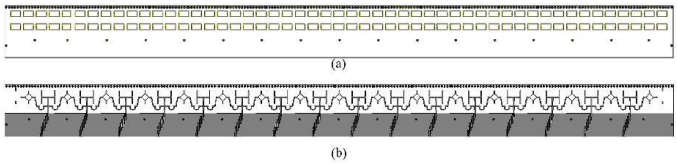

Fig. 14. 16-element phased array structure

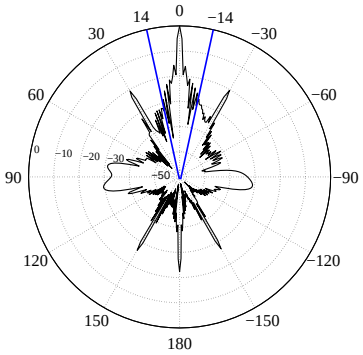

Fig. 15. 16-element phased array pointing to 0°

IV. 16-ELEMENT PHASED ARRAY BEAM STEERING

The 16-element phased array antenna (see Fig. 14) was optimised and designed based on the results achieved for a single element prototype. The steering capability of the phased array antenna was tested in CST by applying progressive phase shift to the 16-element phased array antenna elements. The phased array antenna was nominally steered to 0°,10° and 14°. As Fig. 15 and Fig. 16 respectively indicate by pointing to 0° and 10° there is no grating lobe in the phased array field of view ($\pm$ 14°) as expected. As mentioned the grating lobes are expected to appear at the far edge of the field of view, either at -14° while pointing to +14°. As Fig. 17 illustrates the by steering the beam to +14° degree, there is no grating lobe as a result of using proposed overlapped subarray phased array with Diamond Two-in Two-out splitter. In this case, the grating lobe is appeared outside the visible region of the phased array

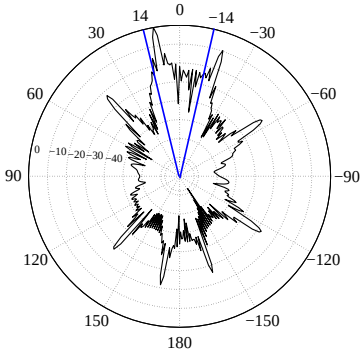

Fig. 16. 16-element phased array pointing to 10°

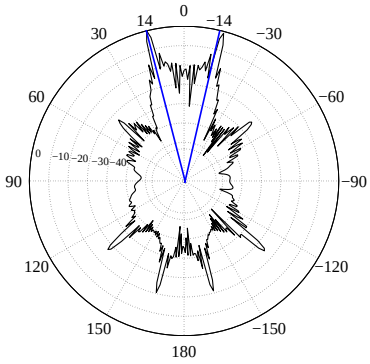

Fig. 17. 16-element phased array pointing to 14°

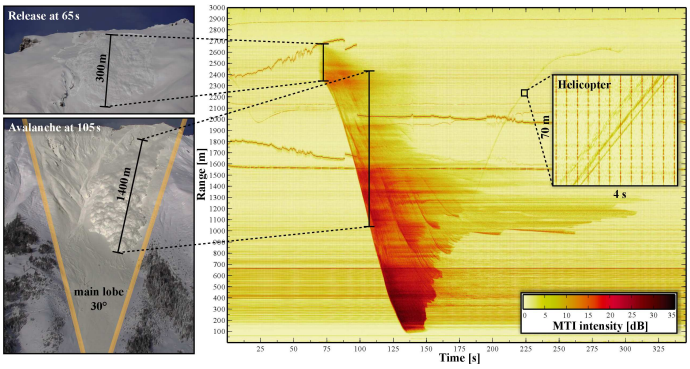

Fig. 18. Radar image of a large powder snow avalanche. Beside this complex, distributed target, a helicopter can be identified.

A. full-scale avalanche results

The proposed 16-element phased array antenna was fabricated and deployed at VDLS. Therefore,to show the functionality and the capability of the proposed phased array antenna to produce high resolution image of the snow avalanche, the preliminary results from the large avalanche which was artificially triggered triggered on 18th of January 2016 is presented. The data processing steps which include chirp extraction, spectrum calculation and moving target identification (MTI) are described in detail in [24]. The MTI is shown in dB normalized to the MTI background. The signature of the moving helicopter as a point target is also captured by the developed phased array system which confirms that the proposed phased array antenna can be used for high resolution imaging. As Fig.18 illustrates, the phased array radar system captures the full avalanche, which is a complex, distributed target directly from the release of an approximately 300 by 300 m snow slab. Although most of the dynamically important flow features are obscured in the visual spectrum under a massive powder snow cloud, the phased array radar system directly images the denser flow features beneath it. Therefore, 16-element phased array FMCW radar gives a comprehensive view with unprecedented spatio-temporal details into large mass movements.

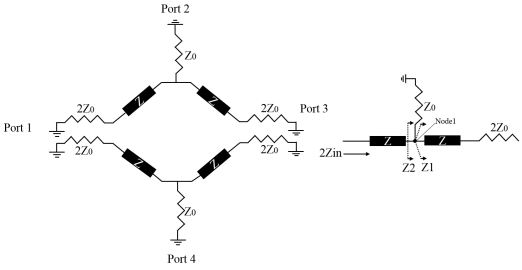

Fig. 19. The equivalent circuit of the Diamond two-in two-out power splitter. The right circuit shows the equivalent circuit of the upper half of the Diamond splitter

V. DISCUSSION

A. diamond two-in two-out splitter mathematical analysis

The Diamond Two-in Two-out splitter behaviour has been mathematically analysed based on transmission line principles. Fig. 19 indicates the equivalent circuit model of the Diamond Two-in Two-out power splitter. Assuming, the power splitter is fed using a single AC power supply at one of the four ends while the other ends are terminated to 50 Ω matched load. Also, for ease of analysis the Z0 characteristic impedance transmission line is considered as two parallel 2Z0 and the junction between the transmission lines is considered as node1. The input impedance at node1 (Z1) is defined as shown in Equation (4, 5 and 6), which is in parallel with Z0 Thus, the input impedance at the feed point can be determined based on transmission line fundamentals as well as reflection and transmission coefficient, see Equation (7) Moreover, by assuming P0 and P1 is the amount of power which travels through port2 and port3 respectively. The S-parameter values can be determined as illustrated by Equation (8), Equation (9) and Equation(10).

$$Z_1 = Z\left(\frac{2Z_0 \tan\beta\ell + jZ\tan\beta\ell}{Z\tan\beta\ell + j2Z_0\tan\beta\ell}\right) \tag{4}$$

$$Z_2 = Z_0 || Z_1 = \frac{Z_0 Z_1}{Z_0 + Z_1} \tag{5}$$

$$Z_{in} = \frac{Z}{2}\left(\frac{Z_2 \tan\beta\ell + jZ\tan\beta\ell}{Z\tan\beta\ell + jZ_2\tan\beta\ell}\right) \tag{6}$$

$$\Gamma_{in} = \frac{Z_{in} - \bar{Z}_0}{Z_{in} + \bar{Z}_0}, \mid T_{in} \mid^2 = 1 - \mid \Gamma_{in} \mid^2 \tag{7}$$

$$P_0 = \frac{V^2}{Z_0}, P_1 = \frac{V^2\,\mathrm{Re}(Z_1)}{\mid Z_1 \mid^2} \tag{8}$$

$$\mid S21 \mid^2 = \frac{\mid T_{in} \mid^2}{2} \times \frac{P_0}{P_0 + P_1} \tag{9}$$

$$\mid S31 \mid^2 = 2\frac{\mid T_{in} \mid^2}{2} \times \frac{P_1}{P_0 + P_1} \tag{10}$$

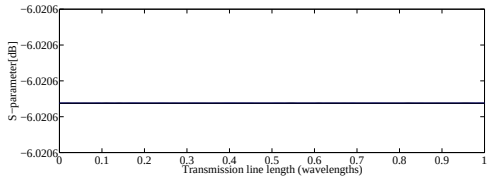

Fig. 20. The Diamond two-in two-out splitter s-parameter response using 100Ω transmission lines. In this case all s_{11}, s_{21} and s_{31} are equal

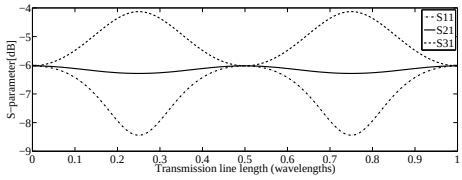

Fig. 21. The Diamond two-in two-out splitter s-parameter response using 78Ω transmission lines.

B. diamond two-in two-out splitter special cases

In the previous section the Diamond Two-in Two-out power splitter general response was discussed using transmission line equations. Therefore, to validate the theoretical results three different transmission line impedances were considered which are 100Ω, 150 Ω and 78 Ωand by varying the transmission line length as a fraction of wavelength the S-parameters are obtained using Matlab software. In the case that the transmission lines impedance is 100 Ω the S_{11}, S_{21} and S_{31} values are equal to 6.025 dB as expected and they are also independent of the transmission line length and precisely the quarter of the input power reaches to each end of the power splitter Fig. 20. However, there is a small variation in S-parameter values (i.e. S_{11}, S_{21} and S_{31}) when 78Ω and 150Ω impedance values is used for the transmission lines which is obviously due to impedance mismatch and the equivalent impedance of each of two parallel transmission lines are 39 Ω and 75 Ω respectively. As Fig. 21 illustrates the S_{11} value for 78 Ω transmission lines varies between approximately -4dB to -6 dB. As it can be realized at λ/4 and 3λ/2 is equal to -4 and at 0, λ/2 and λ is -6 dB. Also, the S21 value is approximately -6 dB along the wavelength and the S_{31} value also fluctuates between -6 dB to -8.5 dB. In this case at λ/4 and 3λ/2 the S_{31} value is equal to -8.5 dB and at 0, λ/2 and λ is equal to -6dB. Moreover, in the case where 150Ω transmission lines are used, as Fig. 22 illustrates, the S_{11} value fluctuates between the -3 dB to -6 dB and at λ/4 and 3λ/2the s_{11} value is -3dB and at 0, λ/2 and λ is -6d B. Also the S_{21} value is approximately -6dB along the wavelength, however, the S_{31} value fluctuates between -6 dB to -11 dB. So, as it can be realized the S_{31} value at λ/4 and 3λ/2 is -11 dB while at 0, λ/2 and λ is -6dB. According to above discussion and the FMCW radar required specifications the Two-in Two-out power splitter with 100Ω transmission lines were used to be able to uniformly distribute power to the each port of the splitter.

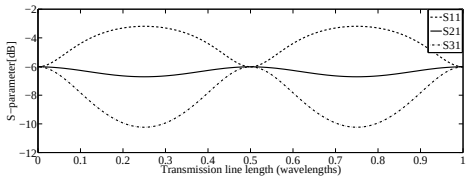

Fig. 22. The Diamond two-in two-out splitter s-parameter response using 150Ω transmission lines.

C. Two-in Two-out splitter using lossy transmission lines

In previous section analysis, lossless transmission lines have been considered for the Diamond two-in two-out splitter. Thus, to consider the transmission line and substrate losses the Diamond splitter has been designed and simulated in CST using 100Ω lossy microstrip transmission lines mounted on Duriod 5880 substrate. This is to thoroughly comprehend the actual behaviour of the power splitter in reality. As known the length of the microstrip transmission line is an important factor in impedance matching. Therefore, by varying the 100Ωlength from 0 to full-wavelength(λ) the optimum length of the transmission line can be achieved to deliver quarter of the input power to each end of the power splitter and as Fig. 23 illustrates to obtain approximately S11=S41=S31= -6dB the transmission lines length (ℓ) should be 15 mm $\prec\ell\prec$ 20 mm. The angle between the transmission lines of the power splitter may also have some effect on the S-parameter values. Therefore, by varying the angle between the 100Ω transmission lines while their lengths are fixed, the effects of the angle on S-parameter can be deduced. As Fig. 24 three different Diamond dividers with different angles between their transmission lines have been modelled. Thus, in the case where α=51.252°, β=128.75° the S_{11}, S_{41} and S_{31} values are approximatively -6.26 dB, -6.24 dB and -6.34 dB respectively across the whole bandwidth, see Fig.25. Moreover, where α=17.10° and β=162.897° the S_{11}, S_{41} and S_{31} values are approximatively -6.4 dB, -6.3 dB and -6.15 dB, respectively, Fig. 26. Ultimately, where there approximately 90° between the transmission lines the S_{11}, S_{41} and S_{31} values are -7.1dB, -6.4dB and -6.2 dB respectively, Fig. 27 As it can be realized from the results the lowest value of S_{11} was achieved in the case where α and β are equal to 90°, in other words as β decreases the S_{11} also decreases and more amount of the power reflects back.

VI. CONCLUSIONS

A phased array FMCW radar system has been described based on a fully populated, regularly spaced phased array antenna using an overlapped sub-array technique to achieve spatial anti-alias filtering. This technique allows suppression of grating lobes by means of a sub-array width that exceeds its spacing, hence resulting in a disproportionally narrower beamwidth. In addition, power distribution network which consists of a Two-in Two-out power splitter which has four ports to divide quarter of the power equally among the ports has been developed. The power is divided equally by using four of two-parallel 100Ω transmission lines in series with

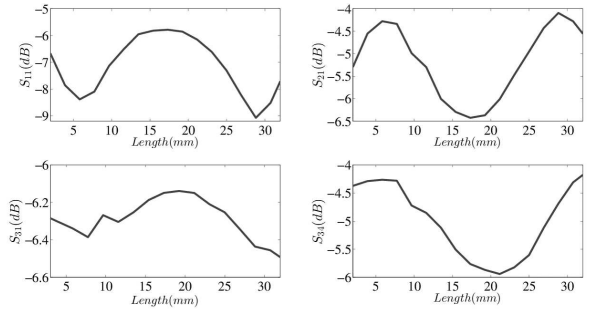

Fig. 23. S-parameter response of the diamond power splitter at 5.3GHz by varying the length of the lossy transmission lines to a full-wavelength (38mm)

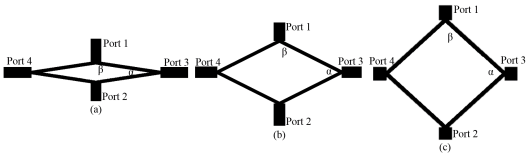

Fig. 24. Two-in two-out splitter with different angles between transmission lines.a)α=17.10°, β=162.897° b)α=51.252°, β=128.75° c)α=84.52°, β=95.46°

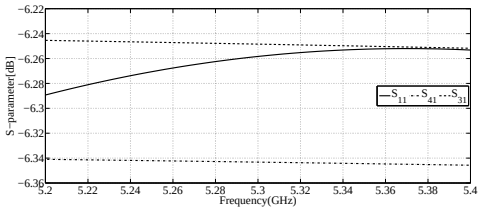

Fig. 25. S-parameter values of the case where α=51.252°, β=128.75°

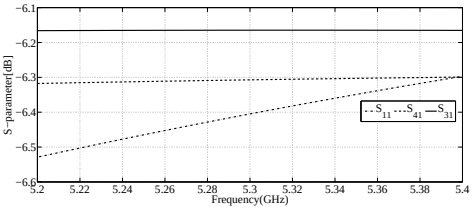

Fig. 26. S-parameter values of the case where α=17.10° and β=162.897°

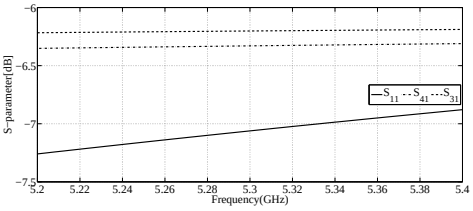

Fig. 27. S-parameter values of the case where α=β=90 °

50Ω transmission line in a diamond orientation. By using the Two-in Two-out power splitter the required amount of power was delivered to the overlapping elements in the phased array structure to reduce the phased array sidelobe level. The results

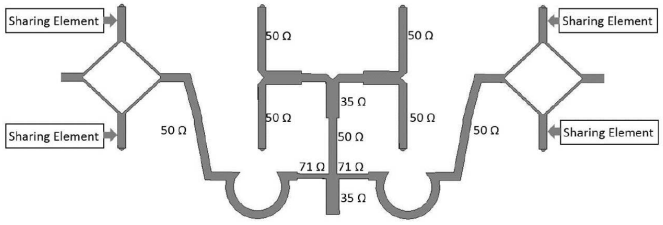

Fig. 28. This picture indicates the feed network transmission line impedances. In this design the 35 Ω and 71 Ω transmission lines are quarter-wavelength.

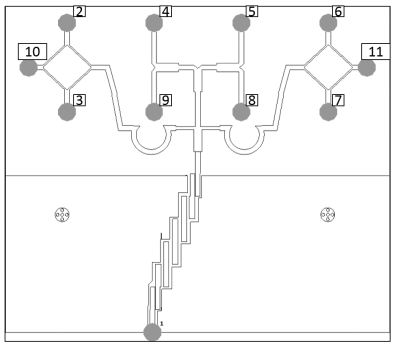

Fig. 29. Above picture indicates the phased array ports

achieved in both simulation and measurement indicate the potential of producing high resolution, unambiguous image of snow avalanches. It is expected that the techniques used in this work will have a range of wider applications

APPENDIX A
PHASED ARRAY FEED NETWORK

Fig. 28 indicates the transmission line impedances of the phased array feed network.

APPENDIX B
PHASED ARRAY PORTS

Fig. 29 indicates the phased array feed network ports used to determine phases.

ACKNOWLEDGEMENT

The authors would like to thank TrackWise, Uk for manufacturing the phased array antenna.

REFERENCES

[1] G. W. Stimson, *Introduction to airborne radar*. SciTech Pub., 1998.
[2] R. C. Hansen, *Phased array antennas*. John Wiley & Sons, 2009, vol. 213.
[3] R. Haupt, "Reducing grating lobes due to subarray amplitude tapering," *IEEE transactions on antennas and propagation*, vol. 33, no. 8, pp. 846–850, 1985.
[4] A. P. Goffer, M. Kam, and P. R. Herczfeld, "Design of phased arrays in terms of random subarrays," *IEEE transactions on Antennas and Propagation*, vol. 42, no. 6, pp. 820–826, 1994.
[5] M. G. Bray, D. H. Werner, D. W. Boeringer, and D. W. Machuga, "Optimization of thinned aperiodic linear phased arrays using genetic algorithms to reduce grating lobes during scanning," *IEEE Transactions on antennas and propagation*, vol. 50, no. 12, pp. 1732–1742, 2002.

[6] R. L. Haupt, "Optimized weighting of uniform subarrays of unequal sizes," *IEEE Transactions on Antennas and Propagation*, vol. 55, no. 4, p. 1207, 2007.

[7] P. Brennan, A. Narayanan, and R. Benjamin, "Grating lobe control in randomised, sparsely populated mimo radar arrays," *IET Radar, Sonar & Navigation*, vol. 6, no. 7, pp. 587–594, 2012.

[8] G.-L. Huang, S.-G. Zhou, T.-H. Chio, H.-T. Hui, and T.-S. Yeo, "A low profile and low sidelobe wideband slot antenna array feb by an amplitude-tapering waveguide feed-network," *IEEE Transactions on Antennas and Propagation*, vol. 63, no. 1, pp. 419–423, 2015.

[9] D. Gray, J. W. Lu, and D. V. Thiel, "Electronically steerable yagi-uda microstrip patch antenna array," *IEEE Transactions on antennas and propagation*, vol. 46, no. 5, pp. 605–608, 1998.

[10] J. Langley, P. Hall, and P. Newham, "Balanced antipodal vivaldi antenna for wide bandwidth phased arrays," *IEE Proceedings-Microwaves, Antennas and Propagation*, vol. 143, no. 2, pp. 97–102, 1996.

[11] Y. Yusuf and X. Gong, "A low-cost patch antenna phased array with analog beam steering using mutual coupling and reactive loading," *IEEE Antennas and Wireless Propagation Letters*, vol. 7, pp. 81–84, 2008.

[12] A. A. Eldek, "Design of double dipole antenna with enhanced usable bandwidth for wideband phased array applications," *Progress In Electromagnetics Research*, vol. 59, pp. 1–15, 2006.

[13] R. C. Johnson and H. Jasik, "Antenna engineering handbook," *New York, McGraw-Hill Book Company, 1984, 1356 p. No individual items are abstracted in this volume.*, vol. 1, 1984.

[14] C. Wood, "Improved bandwidth of microstrip antennas using parasitic elements," *Microwaves, Optics and Antennas, IEE Proceedings H*, vol. 127, no. 4, pp. 231–234, 1980.

[15] K.-L. Wong and W.-H. Hsu, "A broad-band rectangular patch antenna with a pair of wide slits," *IEEE Transactions on Antennas and Propagation*, vol. 49, no. 9, pp. 1345–1347, 2001.

[16] G. Rafi and L. Shafai, "Broadband microstrip patch antenna with v-slot," *IEE Proceedings-Microwaves, Antennas and Propagation*, vol. 151, no. 5, pp. 435–440, 2004.

[17] J.-Y. Sze and K.-L. Wong, "Slotted rectangular microstrip antenna for bandwidth enhancement," *IEEE transactions on antennas and propagation*, vol. 48, no. 8, pp. 1149–1152, 2000.

[18] D. M. Pozar, *Microwave engineering*. John Wiley & Sons, 2009.

[19] M. A. Tanha, P. V. Brennan, and M. Ash, "Phased array antenna for avalanche fmcw radar," in *2013 Loughborough Antennas Propagation Conference (LAPC)*, Nov 2013, pp. 51–55.

[20] M. A. Tanha, M. Ash, and P. V. Brennan, "Phased-array antenna feed network for geophysical fmcw radar," in *Antennas and Propagation (EuCAP), 2014 8th European Conference on*. IEEE, 2014, pp. 1847–1851.

[21] D. Sinnott and G. Haack, "The use of overlapped subarray techniques in simultaneous receive beam linear arrays," (Defence Technical Information Center)DTIC Document, Tech. Rep., 1984.

[22] C. A. Balanis, *Antenna theory: analysis and design*. John Wiley & Sons, 2016.

[23] S. Xiao, B.-Z. Wang, W. Shao, and Y. Zhang, "Bandwidth-enhancing ultralow-profile compact patch antenna," *IEEE transactions on antennas and propagation*, vol. 53, no. 11, pp. 3443–3447, 2005.

[24] A. Köhler, J. McElwaine, B. Sovilla, M. Ash, and P. Brennan, "The dynamics of surges in the 3 february 2015 avalanches in vallée de la sionne," *Journal of Geophysical Research: Earth Surface*, vol. 121, no. 11, pp. 2192–2210, 2016.